Indian Journal of Natural Products and Resources
Vol. 17(3), September 2026, pp 412-429
DOI: 10.56042/ijnpr.v17i3.22565

Mechanism of action of triterpenoid saponins from *Palaquium formosanum* for prostate cancer treatment: Insights from network pharmacology, molecular docking, and dynamics simulations

Hung Duc Nguyen*
Faculty of Biology, Thai Nguyen University of Education, Thai Nguyen, 24124, Vietnam

Received 09 August 2025; revised received 30 July 2026; accepted 03 August 2026

Prostate cancer continues to pose a formidable global health challenge, driving the need for innovative, low-toxicity therapeutic strategies. Natural compounds from traditional herbal origins, notably triterpenoid saponins, demonstrate promise in cancer care by curbing proliferation, triggering apoptosis, and influencing critical signaling pathways. This investigation delved into the mechanism of triterpenoid saponins from *Palaquium formosanum* as potential anti-prostate cancer agents, targeting the myeloid cell leukemia-1 protein (MCL-1, protein ID: 6QGG), with insights derived from network pharmacology, molecular docking, and molecular dynamics simulations. Network pharmacology analysis identified key molecular targets and pathways, providing a comprehensive framework for understanding the saponins' biological impact. Molecular docking revealed that CPD1 and CPD5 exhibit enhanced binding affinities compared to 5FU, suggesting their ability to modulate apoptosis resistance. Molecular dynamics simulations further confirmed stable interactions, with parameters including RMSD, RMSF, Rg, Hbonds, and SASA reinforcing the robustness of the complexes. These findings position CPD1 and CPD5 as promising MCL-1 inhibitors for prostate cancer intervention. Additionally, they establish a foundation for designing novel derivatives with improved potency and safety profiles, awaiting validation through *in vitro* and *in vivo* studies.

Keywords: Anti-apoptosis, Computational chemistry, *Palaquium formosanum*, Prostate cancer, Saponins

IPC code; Int. cl. (2021.01)– A61K 36/00, A61P 35/00

Introduction

Prostate cancer is a significant global health issue for men, with over 1.4 million new cases and 396,792 deaths in 2022[1]. The primary focus of prostate cancer research remains the development of effective prevention and treatment strategies, particularly for metastatic prostate cancer. This includes exploring new therapies and improving existing ones to address the challenges of advanced disease and its impact on patient outcomes. The prevalence of prostate cancer is indeed associated with hereditary factors, age, and genomic alterations[2]. Specifically, family history, advanced age, and specific gene mutations play a role in increasing a man's risk of developing prostate cancer. Androgen deprivation therapy, also known as hormone therapy, remains the primary treatment for metastatic prostate cancer[3]. However, while chemotherapy drugs can be effective in cancer treatment, it is crucial to acknowledge and address the serious side effects they can cause[4]. These adverse reactions can significantly impact a patient's quality of life and should not be overlooked. Consequently, sustained investigations and interdisciplinary partnerships remain essential for advancing therapeutic strategies and clinical results in lung cancer management. Such efforts encompass formulating innovative treatments, refining early diagnostic techniques, and promoting fair healthcare accessibility. Integration of novel pharmacological agents with conventional therapies and immunotherapeutic modalities represents a viable strategy for mitigating drug resistance and enhancing clinical results in patients[5].

Bioactive compounds obtained from traditional medicines exhibit the capacity to elicit apoptosis and alternative modes of programmed cellular demise in neoplastic cells. Such multifaceted mechanisms present a compelling strategy for oncological intervention, with the potential to surmount certain constraints associated with standard chemotherapeutic regimens, which predominantly depend on apoptosis

*Correspondent author
Email: hungnd@tnue.edu.vn

activation[6]. Triterpenoid saponins, a class of plant-derived compounds, exhibit potential anticancer properties by inducing apoptosis in cancer cells through various mechanisms, including targeting signaling pathways involved in cell survival, proliferation, and inflammation[7]. Consequently, triterpenoid saponins exhibit substantial potential as therapeutic agents for prostate cancer management, attributed to their capacity to induce apoptosis within cancer cells[8–10]. *Palaquium formosanum*, rich in saponins, is a promising candidate for treating prostate cancer (PC-3 cell lines)[11]. However, the fine details at the molecular level, especially using advanced computational techniques, are not fully understood. Thus, the present study aimed to explore the anti-prostate cancer activity of triterpenoid saponins isolated from *P. formosanum* by using a comprehensive set of computational techniques to better understand how these compounds interact with their targets and to predict their behaviour within a biological system. These results constitute a basis for subsequent experimental verification and enhancement of these compounds as potent and reliable interventions for prostate cancer, contingent upon additional *in vitro* and *in vivo* examinations.

Materials and Methods

Preparation of selected steroidal saponins

The triterpenoid saponins from *P. formosanum* possessing cytotoxic activity against human prostate cancer (PC-3 cell line) were collected from a literature source[11]. For details, these selected triterpenoid saponins, including 3'''-*O*-rhamnopyranosyl-arganin C (CPD1), arganin C (CPD2), butyrosides B (CPD3), 3'-*O*-glucosyl-arganin C (CPD4), 3'-*O*-glucosyl-3'''-*O*-rhamnosyl-arganin C (CPD5), mi-saponin A (CPD6), mimusopsin (CPD7), 6β-hydroxy-conyzasaponin N (CPD8), mi-saponins B (CPD9), mi-saponins C (CPD10) have molecular formulas of $C_{64}H_{104}O_{32}$, $C_{58}H_{94}O_{28}$, $C_{57}H_{92}O_{28}$, $C_{64}H_{104}O_{33}$, $C_{70}H_{114}O_{37}$, $C_{58}H_{94}O_{27}$, $C_{64}H_{104}O_{32}$, $C_{62}H_{100}O_{31}$, $C_{63}H_{102}O_{31}$, $C_{64}H_{104}O_{32}$, and molecular weights of 1384.6511, 1238.5932, 1224.5775, 1400.6460, 1546.7039, 1222.5982, 1384.6511, 1340.6249, 1354.6405, 1384.6511 *m/z*, respectively (Fig. 1). Two-dimensional ligand structures were generated in .sdf format through ChemDraw Prime v23.1 (Perkin Elmer, USA), followed by conversion into three-dimensional .pdb format via Biovia Discovery Studio Visualizer v24.1 (Dassault Systèmes BIOVIA, USA). Polar hydrogen atoms and Gasteiger partial charges were subsequently incorporated, and every torsion angle was rendered rotatable through AutoDock Tools 1.5.7 (Center for Computational Structural Biology, USA). The 2D structure of the comparative reference, 5FU (PubChem CID: 3385), possessing molecular formula of $C_4H_3FN_2O_2$ and molecular weight of 130.0179 *m/z*, was obtained from the PubChem database in .sdf format (https://pubchem.ncbi.nlm. nih.gov) and further converted to .pdb format using Biovia Discovery Studio Visualizer.

Molecular target prediction

The two-dimensional structural similarity between each drug and the ligand set of each target was assessed as an expectation value (E-value) through the Similarity Ensemble Approach (SEA)[12]. The SMILES strings for the selected triterpenoid saponins were acquired and submitted to the SEA database, with *Homo sapiens* designated as the target organism to ensure predictions pertinent to human biology. This methodology supported recognizing biological processes potentially impacted by these triterpenoid saponins, establishing a basis for additional inquiry into their mechanisms of action.

Prediction of protein–protein interaction network

The protein-protein interaction (PPI) networks for the selected triterpenoid saponins were examined using the STRING database (https://string-db.org)[13]. Potential target proteins ascertained from the SEA analysis were incorporated into STRING, with *Homo sapiens* indicated as the reference organism to maintain relevance to humans. These networks prove indispensable for interpreting the potential mechanisms of action of the compounds within a systems biology framework.

Biosignaling network prediction

The X2K Web platform was utilised to examine upstream regulatory networks linked to target proteins of triterpenoid saponins, integrating predictive insights and molecular pathway analysis[14]. X2K aggregates information on transcription factors, kinases, and protein-protein interactions to generate regulatory networks for gene sets sourced from SEA and STRING, with *Homo sapiens* specified as the reference species.

Molecular docking

The three-dimensional structures of all chosen triterpenoid saponins were constructed in .pdb format

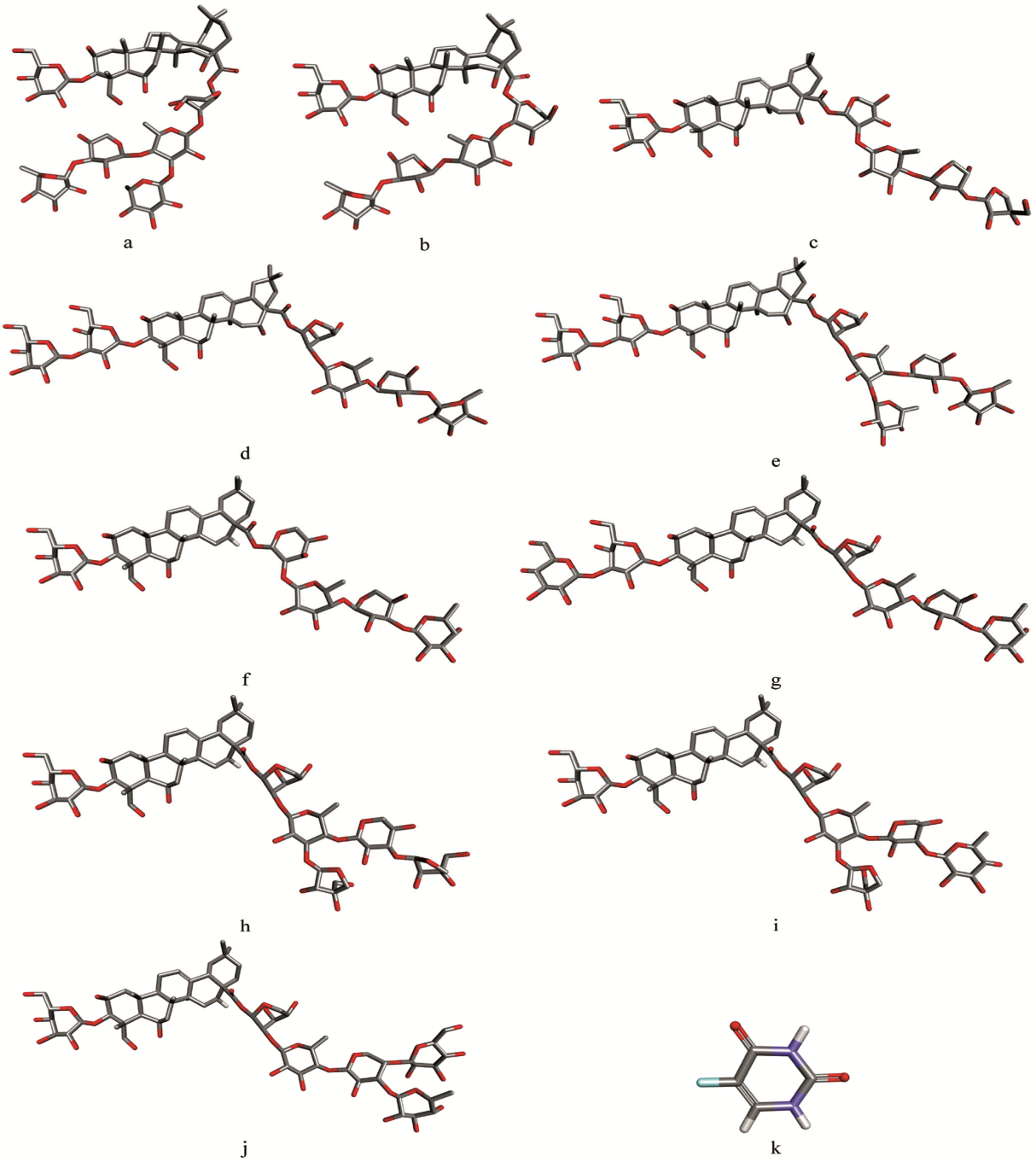

Fig. 1 — 3D structure of the selected triterpenoidsaponins. (a) CPD1, (b) CPD2, (c) CPD3, (d) CPD4, (e) CPD5, (f) CPD6, (g) CPD7, (h) CPD8, (i) CPD9, (j) CPD10, and (k) the comparative reference, 5FU.

through Biovia Discovery Studio Visualizer, with inclusion of solely polar hydrogens and Gasteiger charges, and permission for rotation of all torsions[15]. The three-dimensional configuration of the target Bcl-xL protein (ID: 6QGG) was acquired in .pdb format from the RCSB Protein Data Bank[16]. Evaluation of the structural quality for protein 6QGG occurred via analysis of phi (φ) and psi (ψ) torsion angles employing a Ramachandran plot produced by PROCHECK (Program to Check the Stereochemical Quality of Protein Structures)[17]. Molecular docking between the protein and ligands proceeded with AutoDock Tools. The configuration of the grid involved dimensions of x = 58, y = 72, z = 44,

alongside a spacing of 0.375 Å among grid points. Establishing docking site coordinates occurred at x = -15.618 Å, y = 14.362 Å, and z = -7.312 Å inside the binding pocket of the 6QGG protein. Application of the Lamarckian genetic algorithm facilitated the determination of ligand-protein binding conformations characterised by the lowest energy.

Molecular dynamics simulations

Molecular dynamics simulations of the optimal docked configuration with the 4G3F protein were executed for 100 ns employing GROMACS version 2024.4[18]. The protein configuration underwent refinement via Swiss-PdbViewer to rectify absent atoms and residues[19]. Topologies for ligands were formulated utilising SwissParam[20]. The solvation arrangement incorporated a triclinic simulation box adapted to the protein-ligand complex, applying the SPC water model and supplementing a 0.15 M sodium chloride concentration. Optimisation of the structure and achievement of neutralisation occurred through 50,000 iterations of energy minimisation. For each system, three simulations spanning 100 nanoseconds were implemented, utilising a time step of 2 femtoseconds (0.002 ps), with trajectory records preserved at intervals of 10 ns. Examination of simulation outputs utilised Grace software (Grace Development Team) to quantify metrics including radius of gyration (Rg), root mean square deviation (RMSD), quantity of hydrogen bonds (H-bonds), root mean square fluctuation (RMSF) across residues, and solvent-accessible surface area (SASA). Assessment of conformational stability for the docked entities involved overlay procedures conducted with UCSF Chimera version 1.1[21].

Molecular mechanics generalised born surface area (MMGBSA) analysis

The MMGBSA approach, implemented in gmx_MMPBSA using the charmm36-jul2022.ff force field, was applied to calculate the binding free energy of the CPD1-6QGG, CPD5-6QGG, and 5FU-6QGG complexes. The Generalised Born model determined the electrostatic solvation energy in a continuum solvent environment, whereas the non-polar solvation energy was assessed through computation of the solvent-accessible surface area. Calculations derived from molecular dynamics simulation trajectories involved the extraction of 125 snapshots at 80 ps intervals across the 80 ns duration[22].

Results and Discussion

Molecular target, protein interaction, and biosignaling network

A Ramachandran plot was generated through the PROCHECK software to assess the stereochemical accuracy of the refined 6QGG protein structure, identified as MCL-1, a pivotal component in the apoptosis regulation pathway associated with prostate cancer cell viability. This plot segments the conformational domain into specific zones, determined by the distribution of Φ and Ψ dihedral angles, representing the thermodynamically stable configurations of amino acid residues based on a high-resolution protein structure dataset. The Φ angles align along the x-axis, and the Ψ angles along the y-axis, delineating residue orientations. For the 6QGG structure, the evaluation indicated that 96.00% of residues, excluding glycine and proline, fall within the most favoured regions (A, B, L), totaling 121 residues, while 4.00% occupy the additionally allowed regions (a, b, l, p), amounting to 5 residues. No residues were observed in the generously allowed regions (~a, ~b, ~l, ~p) or disallowed regions, with counts of 0 residues each, based on a total of 126 non-glycine and non-proline residues, constituting 100.00% of this group. The complete structure consists of 140 residues, comprising 3 terminal residues (excluding glycine and proline), 10 glycine residues (represented as triangles), and one proline residue (Fig. 2). Reference to an analysis of 118 structures with resolutions of at least 2.0 Angstroms and R-factors not exceeding 20% suggests that a high-quality model typically exhibits over 90% of residues in the most favored regions, a criterion met by the 6QGG structure.

The observed distribution corresponds to the standards for a structurally robust model, wherein at least 90% of residues are anticipated to reside in the most favoured regions, based on the evaluation of 118 structures exhibiting a resolution of 2.0 Å or better and an R-factor below 20%. The absence of residues in disallowed regions (0.0%) for the 6QGG structure reinforces its conformational integrity, rendering it an appropriate framework for molecular docking and simulation analyses. This structural stability augments the precision of forecasting interactions between triterpenoid saponins and the MCL-1 binding site, thereby supporting the evaluation of their capacity to modulate the apoptosis pathway and their effectiveness as potential therapeutic agents against prostate cancer cells.

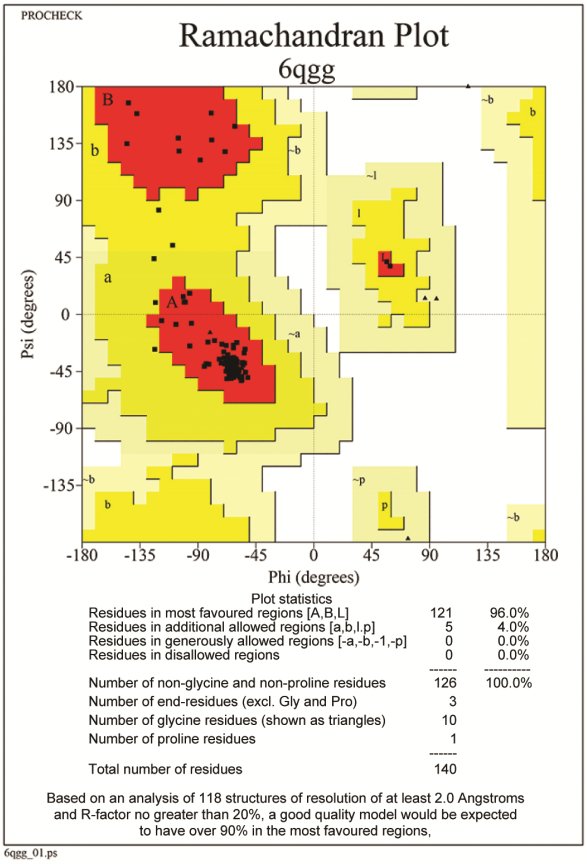

Fig. 2 — Ramachandran plot of energy-minimized predicted structures of 6QGG.

The molecular target predictions outlined in Table 1 reveal associations between the identified triterpenoid saponins and numerous key human proteins, including CD81 (CD81 antigen), FGF1 (Fibroblast growth factor 1), F3 (Tissue factor), PTPN1 (Tyrosine-protein phosphatase non-receptor type 1), FGF2 (Fibroblast growth factor 2), PTPN2 (Tyrosine-protein phosphatase non-receptor type 2), LGALS9 (Galectin-9), VEGFA (Vascular endothelial growth factor A), AKR1B10 (Aldo-ketoreductase family 1 member B10), and NFE2L2 (Nuclear factor erythroid 2-related factor 2), alongside other potential candidates. Notably, NFE2L2 emerges as a significant protein involved in cellular oxidative stress responses, while targets such as FGF1, FGF2, and VEGFA indicate potential roles in angiogenesis and cellular proliferation pertinent to cancer progression. Within the context of the current study, which targets the inhibition of apoptosis-related pathways in prostate cancer, MCL-1 (corresponding to 6QGG) does not appear directly within the SEA results but gains prominence through subsequent analyses employing STRING and X2K. This observation highlights MCL-1's critical function in regulating survival and resistance to apoptosis in prostate cancer cells, positioning it as a central target for further investigation via molecular docking and network-based approaches.

Table 1 — Molecular target prediction of selected triterpenoid saponins

N°	Target gene	Description	P-value	MaxTC
CPD1	CD81	CD81 antigen	1.97E-44	0.35
	FGF1	Fibroblast growth factor 1	2.22E-16	0.29
	F3	Tissue factor	1.52E-13	0.57
	PTPN1	Tyrosine-protein phosphatase non-receptor type 1	1.52E-07	0.4
	FGF2	Fibroblast growth factor 2	5.24E-07	0.28
	PTPN2	Tyrosine-protein phosphatase non-receptor type 2	8.58E-07	0.41
	LGALS9	Galectin-9	2.02E-06	0.28
CPD2	CD81	CD81 antigen	1.97E-44	0.35
	FGF1	Fibroblast growth factor 1	1.30E-24	0.3
	F3	Tissue factor	1.52E-13	0.57
	FGF2	Fibroblast growth factor 2	1.61E-13	0.3
	VEGFA	Vascular endothelial growth factor A	6.11E-10	0.3
	PTPN1	Tyrosine-protein phosphatase non-receptor type 1	2.79E-07	0.4
	PTPN2	Tyrosine-protein phosphatase non-receptor type 2	8.58E-07	0.41
CPD3	CD81	CD81 antigen	5.17E-42	0.33
	F3	Tissue factor	3.57E-12	0.54
	FGF1	Fibroblast growth factor 1	1.81E-08	0.28
	FGF2	Fibroblast growth factor 2	6.32E-07	0.28
CPD4	CD81	CD81 antigen	1.35E-43	0.35

(*Contd.*)

Table 1 — Molecular target prediction of selected triterpenoid saponins (*Contd.*)

N°	Target gene	Description	P-value	MaxTC
	FGF1	Fibroblast growth factor 1	2.62E-33	0.31
	FGF2	Fibroblast growth factor 2	1.31E-20	0.31
	VEGFA	Vascular endothelial growth factor A	4.55E-15	0.31
	F3	Tissue factor	1.30E-12	0.56
CPD5	CD81	CD81 antigen	1.35E-43	0.35
	FGF1	Fibroblast growth factor 1	7.65E-25	0.3
	FGF2	Fibroblast growth factor 2	8.18E-14	0.3
	F3	Tissue factor	1.30E-12	0.56
	VEGFA	Vascular endothelial growth factor A	3.74E-10	0.3
CPD6	PTPN2	Tyrosine-protein phosphatase non-receptor type 2	3.24E-28	0.5
	FGF1	Fibroblast growth factor 1	9.92E-25	0.29
	PTPN1	Tyrosine-protein phosphatase non-receptor type 1	1.44E-21	0.49
	F3	Tissue factor	1.11E-16	0.56
	FGF2	Fibroblast growth factor 2	1.69E-13	0.29
	VEGFA	Vascular endothelial growth factor A	6.31E-10	0.29
	AKR1B10	Aldo-keto reductase family 1 member B10	3.36E-07	0.34
	NFE2L2	Nuclear factor erythroid 2-related factor 2	9.89E-06	0.33
CPD7	FGF1	Fibroblast growth factor 1	1.36E-33	0.31
	PTPN2	Tyrosine-protein phosphatase non-receptor type 2	3.28E-26	0.49
	FGF2	Fibroblast growth factor 2	1.00E-20	0.31
	PTPN1	Tyrosine-protein phosphatase non-receptor type 1	4.49E-19	0.48
	F3	Tissue factor	3.33E-16	0.54
	VEGFA	Vascular endothelial growth factor A	3.78E-15	0.31
	AKR1B10	Aldo-keto reductase family 1 member B10	4.50E-07	0.33
CPD8	PTPN2	Tyrosine-protein phosphatase non-receptor type 2	4.56E-21	0.45
	PTPN1	Tyrosine-protein phosphatase non-receptor type 1	6.66E-16	0.47
	F3	Tissue factor	1.11E-15	0.52
	AKR1B10	Aldo-keto reductase family 1 member B10	9.29E-07	0.32
CPD9	PTPN2	Tyrosine-protein phosphatase non-receptor type 2	8.81E-21	0.47
	PTPN1	Tyrosine-protein phosphatase non-receptor type 1	3.89E-15	0.46
	F3	Tissue factor	1.07E-14	0.51
	AKR1B10	Aldo-keto reductase family 1 member B10	1.01E-06	0.31
CPD10	PTPN2	Tyrosine-protein phosphatase non-receptor type 2	3.18E-25	0.47
	FGF1	Fibroblast growth factor 1	4.52E-24	0.29
	PTPN1	Tyrosine-protein phosphatase non-receptor type 1	4.75E-18	0.47
	F3	Tissue factor	3.33E-16	0.54
	FGF2	Fibroblast growth factor 2	3.86E-13	0.28
	VEGFA	Vascular endothelial growth factor A	1.15E-09	0.28
	AKR1B10	Aldo-keto reductase family 1 member B10	5.18E-07	0.33

The ten candidate gene products identified through SEA screening (CD81, F3, FGF1, FGF2, PTPN1, PTPN2, LGALS9, VEGFA, AKR1B10, and NFE2L2) were subsequently evaluated for network connectivity to restrict this pool to the most biologically central candidates. The protein-protein interaction network, derived from the STRING database, revealed an intricate web of associations among the predicted molecular targets, with MCL-1, VEGFA, PTPN2, and NFE2L2 emerging as central hubs due to their extensive interconnections (Fig. 3). This finding suggests that these proteins potentially function as key regulators in modulating cellular survival and proliferation mechanisms, particularly in the context of prostate cancer cells. Further analysis of the STRING network, focusing on MCL-1, identified direct interactions with proteins such as AKT1, STAT3, and MAPK1. These associations emphasize

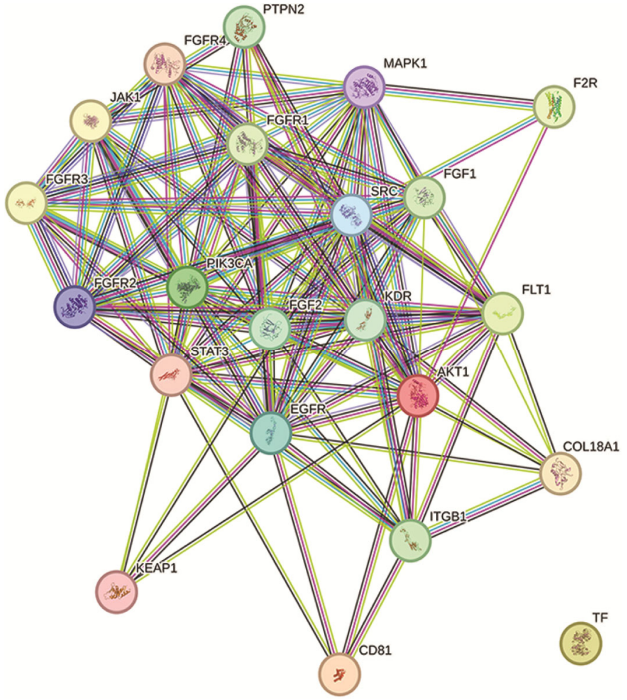

Fig. 3 — Protein-protein interactions of molecular targets of selected triterpenoid saponins.

MCL-1's critical involvement in the apoptosis regulation pathway, where AKT1 contributes to survival signaling through the PI3K/AKT cascade, STAT3 enhances transcriptional activity of anti-apoptotic genes, and MAPK1 supports proliferation via the MAPK/ERK pathway. The inclusion of AKT1 highlights a mechanism linked to apoptosis inhibition, potentially influencing the expression of genes promoting cell survival.

Additional scrutiny uncovered interactions involving VEGFA (Vascular endothelial growth factor A), PTPN2 (Tyrosine-protein phosphatase non-receptor type 2), and FGF1 (Fibroblast growth factor 1), broadening the network's relevance to apoptosis and angiogenesis regulation. VEGFA likely participates in angiogenic processes that intersect with survival signaling, possibly amplifying tumour growth. PTPN2, a phosphatase, may regulate tyrosine kinase signaling pathways that impinge on apoptosis control, while FGF1, a growth factor, suggests a role in cellular proliferation and survival signaling networks pertinent to prostate cancer progression[23]. For compounds interacting with additional targets such as F3 (Tissue factor) and CD81 (CD81 antigen), roles in coagulation (F3) and cell adhesion (CD81) may indirectly contribute to apoptosis modulation by altering cellular microenvironment and signaling dynamics.

The MCL-1 protein, corresponding to the 6QGG structure, emerges as a pivotal upstream regulator absent from the initial SEA dataset yet detected through STRING and X2K analyses. MCL-1's role in suppressing apoptosis, mediated by its interaction with pro-apoptotic proteins such as BAX and BAK, underscores its relevance in sustaining cell survival within prostate cancer cells. This function receives support from additional kinases, including AKT1 and MAPK1, identified in the X2K network, which likely influence apoptosis regulation through survival and proliferation signaling pathways. Transcription factors such as STAT3 and CREB, also elucidated in the X2K analysis, modulate gene expression linked to apoptosis inhibition. Thereby strengthening MCL-1's status as a primary candidate for molecular docking investigations with the studied triterpenoid saponins (Fig. 4). Sub-networks built around the other three hub candidates converged mainly on angiogenic (VEGFA), broader phosphatase (PTPN2), and oxidative-stress (NFE2L2) signaling, connections less specific to apoptosis resistance; this differential convergence, rather than hub status alone, distinguished MCL-1 from the remaining three candidates, supporting selection as the sole target advanced to molecular docking.

The pharmacological mechanism of the triterpenoid saponins has been elucidated through molecular target predictions, protein-protein interaction network analysis, and biosignaling pathway evaluation, establishing a foundation for their incorporation into docking studies targeting MCL-1 (6QGG). The investigation identified AKT1, a key upstream kinase, as an essential regulator in maintaining apoptosis inhibition, providing direct support for docking interactions with the 6QGG protein to attenuate MCL-1 activity (Fig. 5a). MAPK1 and JAK1, identified as prominent nodes within the PPI network, engage in signaling pathways linked to survival and proliferation responses, contributing to cellular conditions that modulate apoptosis regulation, a process validated by docking assessments[24]. VEGFA, noted in the molecular target predictions, may participate in angiogenic signaling, potentially enhancing MCL-1 inhibition through additional regulatory mechanisms, aligning with the docking strategy targeting MCL-1[25]. MCL-1, a kinase implicated in survival signaling within the biosignaling network, likely undergoes inhibition under these conditions, promoting suppression of the

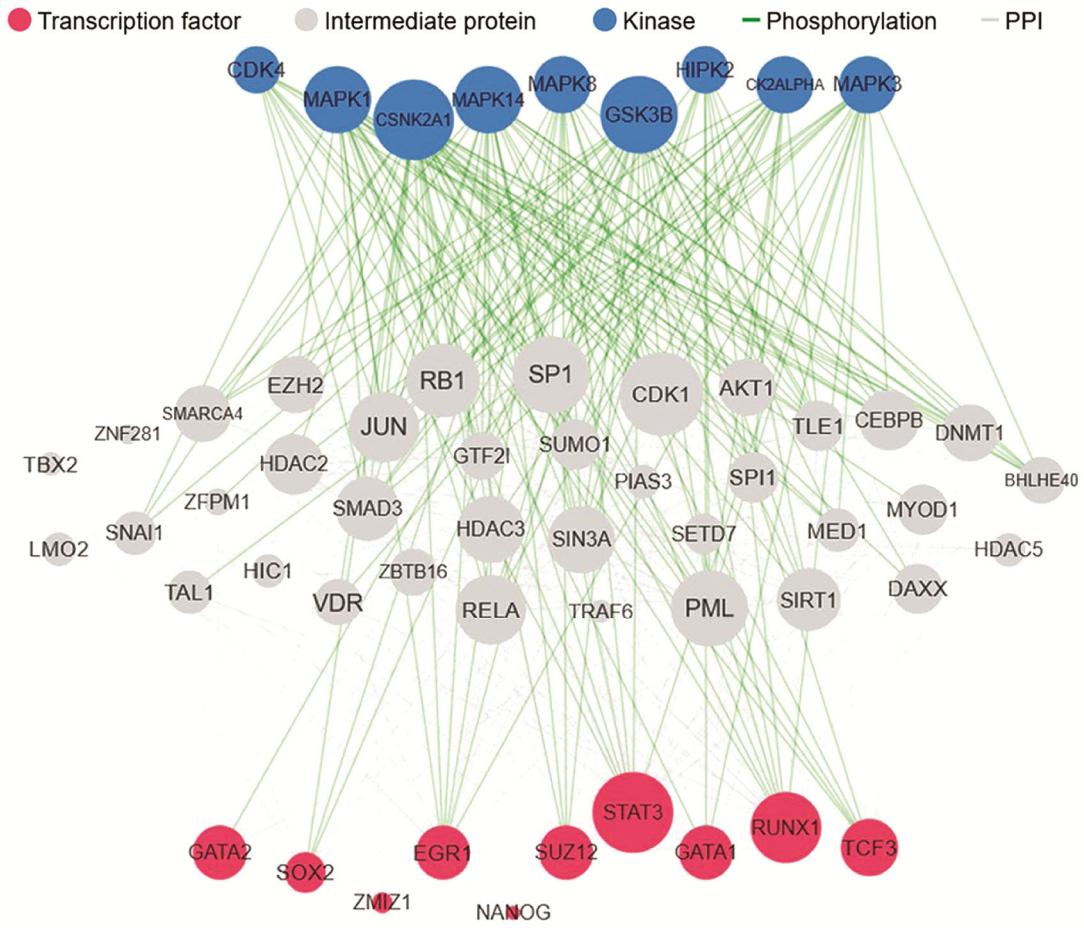

Fig. 4 — Network of kinases and transcription factors linked to molecular targets of selected triterpenoid saponins.

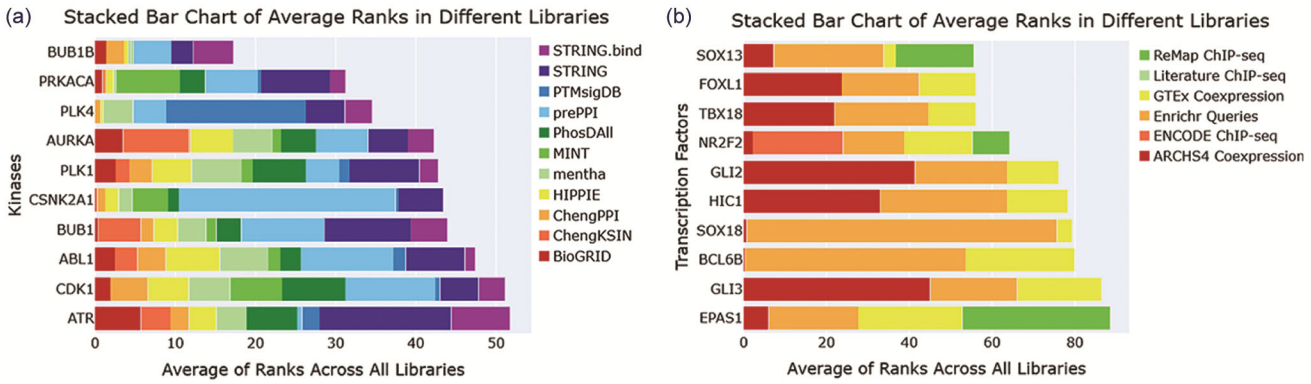

Fig. 5 — Selected triterpenoid saponins associated with (a) kinases and (b) transcription factors average rank across biological libraries.

apoptosis resistance pathway. Transcription factors such as STAT3 and RUNX1, detected through X2K analysis, govern the expression of genes associated with anti-apoptotic and proliferative responses, bolstering the apoptosis modulation pathway addressed by the docking approach (Fig. 5b). Furthermore, NFE2L2, a notable protein in the PPI network and an indicator of oxidative stress response in cancer cells, suggests that triterpenoid saponins may influence metabolic processes, potentially elevating intracellular compound levels and amplifying MCL-1 inhibitory signaling, a hypothesis reinforced by docking into 6QGG. Additional kinases, including CDK1, GSK3B, MAPK14, CSNK2A1, and

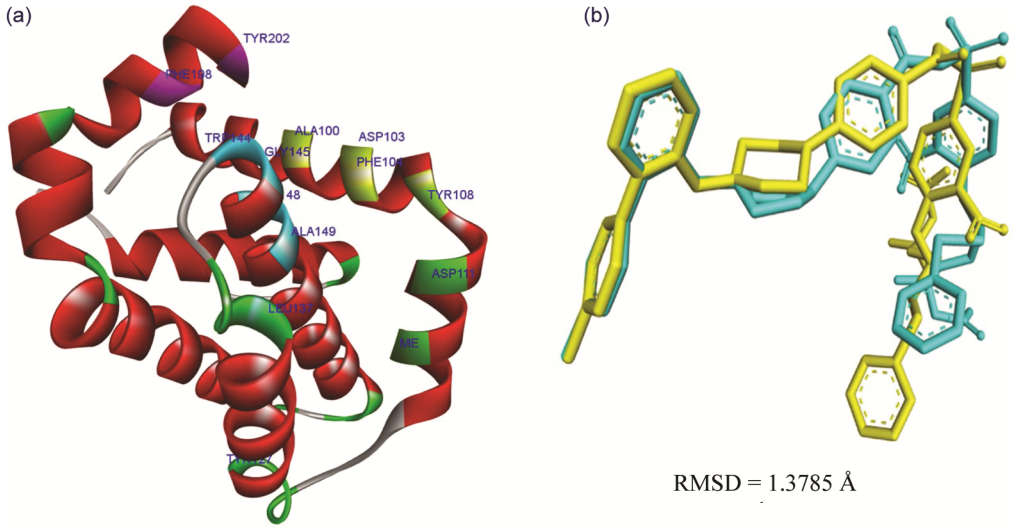

Fig. 6 — (a) Active sites in the 6QGG protein, and the superposition of the docked and (b) original ligands validating the molecular docking protocol (violet = original, cyan = docked).

PIK3CA, along with transcription factors such as EGR1, NFKB1, GATA2, SOX2, and CREB, identified within the X2K network, may participate in the comprehensive regulation of apoptosis signaling and cellular responses, further substantiating the potential therapeutic impact of the triterpenoid saponins in targeting prostate cancer cells.

hese findings corroborate previous studies on regulating survival pathways by natural compounds in cancer cells, where cellular stress responses and transcription factor dynamics are key factors influencing apoptosis pathway activity. The recognition of VEGFA as a potential target from molecular target predictions supports the capacity of the triterpenoid saponins to promote angiogenesis inhibition, an upstream mechanism potentially linked to MCL-1 suppression in prostate cancer cells, a phenomenon further investigated through molecular docking. Nevertheless, NFE2L2, identified within the biosignaling network and noted for its complex role in oxidative stress modulation, indicates a multifaceted regulatory system requiring further investigation to elucidate its impact on PC-3 resistance. The integration of molecular target predictions, protein-protein interaction mapping, and biosignaling network evaluation has thus provided a robust basis for designating 6QGG as the principal docking target, delivering a thorough insight into the therapeutic prospects of these triterpenoid saponins in inhibiting cancer signaling through MCL-1 in prostate cancer cells, with a potential secondary influence on cell survival modulation.

Molecular docking analysis

Molecular docking is a valuable tool in structure-based drug design, enabling the prediction of how small molecules will bind to larger molecules. This prediction involves determining the most likely binding conformation and calculating the free energy of binding, which is crucial for understanding and potentially designing new drugs[26]. This study evaluated the binding energy and interactions between the protein 6QGG and the selected triterpenoid saponins compared to 5FU. Visualisation of the 6QGG protein structure revealed the active sites, including Ala100, Asp103, Phe104, Tyr108, Asp111, Met115, Tyr127, Leu137, Trp144, Gly145, Val148, Ala149, Phe198, and Tyr202 (Fig. 6a). Before conducting docking simulations, validation of the docking protocol for the protein 6QGG becomes imperative through a redocking procedure. This process incorporated the co-crystallized ligand, with outcomes detailed in Fig. 6b. The docking protocol's reliability emerged from an RMSD measurement of 1.3785 Å, supported by the overlay of the native and docked ligands, verifying the precision of the technique. An RMSD threshold below 2 Å is often used as an indicator of a successful docking pose in docking studies[27].

The engagement of the identified triterpenoid saponins within the binding cavities of the protein 6QGG is documented in Table 2. The amino acid residues in these associations, including their exact positions within the ligand-binding region, were determined. Molecular docking elucidated the presence

Table 2 — The interactions between the docked ligands and the protein 6QGG

Docked ligands	Binding energy (kcal/mol)	Hydrogen bond interaction	Van der Waals interaction	Hydrophobic interaction
CPD1	-10.50	Asp103, Arg107, Glu136, Leu137, Gly203	Phe104, Leu106, Asn143, Trp144, Gly145, Arg146, Ala149, Leu201	Tyr108, Val148, Tyr202
CPD2	-9.67	ASp103, Arg107, Tyr108, Asp111	Thr96, Gln99, Phe104, Met115, Val133, Leu137, Asn143, Trp144m Gly145, Val148, Leu201, Gly203	ALa100, Arg146, Tyr202
CPD3	-8.74	Arg107, Val133, Leu137, Leu201, Tyr202	Ala100, Asp103, Phe104, Asp111, Met115, Glu136, Asn143, Trp144, Gly145, Val148, Ala149, Phe198	Tyr108, Arg146, Tyr202
CPD4	-7.45	Asp111, Glu136, Asn143, Gly145, Arg146, Ala149, Phe153, Tyr202	Phe104, Arg107, Met115, Val133, Val134, Leu137, Trp144, Phe150	Tyr108
CPD5	-10.38	Thr96, Gln99, Ala100, Arg107, Tyr108, Asp111, Ala149, Tyr202	Gln95, Leu97, Asp103, Phe104, Phe112, Met115, Val133, Glu136, Leu137, Asn143, Gly145, Phe150, Phe153, Phe198, Leu201, Gly203	Arg146
CPD6	-10.19	Thr96, Ala100, Asp103, Arg107, Tyr108, Asp111, Val133, Glu136, Tyr202	Gln99, Phe104, Met115, Leu137, Asn143, Trp144, Gly145, Ala149, Gly203	Tyr108, Arg146, Tyr202
CPD7	-9.73	Arg107, Tyr108, Asp111 Arg146, Leu201, Tyr202, Gly203	Ala100, Asp103, Phe104, Met115, Val133, Glu136, Leu137, Asn143, Gly145, Val148, Ala149, Phe153	–
CPD8	-8.03	Asp103, Phe104, Asp111, Gly145, Ala149, Leu201, Tyr202	Ala100, Arg107, Leu137, Asn143, Arg146, Val148, Phe153	Tyr108
CPD9	-7.05	Gln99, Asp103, Arg107, Asp111, Gly145	Ala100, Asp102, Phe104, Leu137, Asn143, Val148, Ala149, Phe198, Tyr202, Gly203	Tyr108, Arg146, Tyr202
CPD10	-8.79	Asp103, Arg107, Glu136, Leu137, Gly145	Gln99, Asp111, Met115, Val133, Asn143, Arg146, Val148, Ala149, Gly203	Ala100, Phe104, Tyr108, Tyr202
5FU	-3.50	Asp111, Phe112, Ala149	Phe104, Ser105, Leu137, Glu152, Phe153, Val156	Met115, ALa149

of hydrogen bonding, van der Waals, and hydrophobic interactions between the protein and ligands, with each distinct molecular contact involving the 6QGG amino acids depicted in Fig. 7.

The triterpenoid saponins, specifically CPD1 and CPD5, exhibited prominent interaction profiles with the 6QGG protein, a crucial apoptosis regulator in prostate cancer cells. CPD1 established 16 total interactions including 5 hydrogen bonds (Asp103, Arg107, Glu136, Leu137, Gly203), 8 van der Waals interactions (Phe104, Leu106, Asn143, Trp144, Gly145, Arg146, Ala149, Leu201), and 3 hydrophobic interactions (Tyr108, Val148, Tyr202). Among of these, amino acid residues Asp103, Phe104, Tyr108, Asp111, Met115, Tyr127, Leu137, Trp144, Gly145, Val148, Ala149, Phe198, and Tyr202 are placed at the active sites of the 6QGG protein (Fig. 7a). The binding energy of CPD1 with 6QGG reached at -10.5 kcal/mol.

Likewise, CPD5 formed 25 total interactions with the 6QGG protein including 8 hydrogen bonds (Thr96, Gln99, Ala100, Arg107, Tyr108, Asp111, Ala149, Tyr202), 16 van der Waals interactions (Gln95, Leu97, Asp103, Phe104, Phe112, Met115, Val133, Glu136, Leu137, Asn143, Gly145, Phe150, Phe153, Phe198, Leu201, Gly203) and a hydrophobic interaction (Arg146). Among these, Ala100, Asp103, Phe104, Tyr108, Asp111, Met115, Leu137, Trp144, Gly145, Val148, Ala149, Phe198, and Tyr202 are amino acid residues placed at the active sites of the 6QGG protein (Fig. 7e). The binding energy of CPD5 with 6QGG was -10.38 kcal/mol, indicating considerable stability.

In contrast, 5-Fluorouracil (5FU), employed as a reference compound, established 10 total interactions, with 5 targeting key active sites (Phe104, Asp111, Met115, Leu137, Ala149), including 3 hydrogen bonds (Asp111, Phe112, Ala149), 6 van der Waals interactions (Phe104, Ser105, Leu137, Glu152, Phe153, Val156), and 2 hydrophobic interactions (Met115, Ala149). The binding energy of 5FU with 6QGG was -3.5 kcal/mol (Fig. 7k). Although 5FU demonstrated a degree of interaction, its less negative binding energy and reduced number of interactions

and active site engagements suggest a relatively weaker interaction profile compared to CPD1 and CPD5.

Molecular docking simulations of the triterpenoid saponins with the 6QGG protein unveiled diverse interaction types, encompassing hydrogen bonds, van der Waals forces, and hydrophobic interactions, which collectively bolster the structural integrity of the ligand-protein complex[28]. Hydrogen bonds denote specific, energetically favourable associations involving hydrogen sharing between electronegative atoms such as oxygen or nitrogen. Hydrophobic

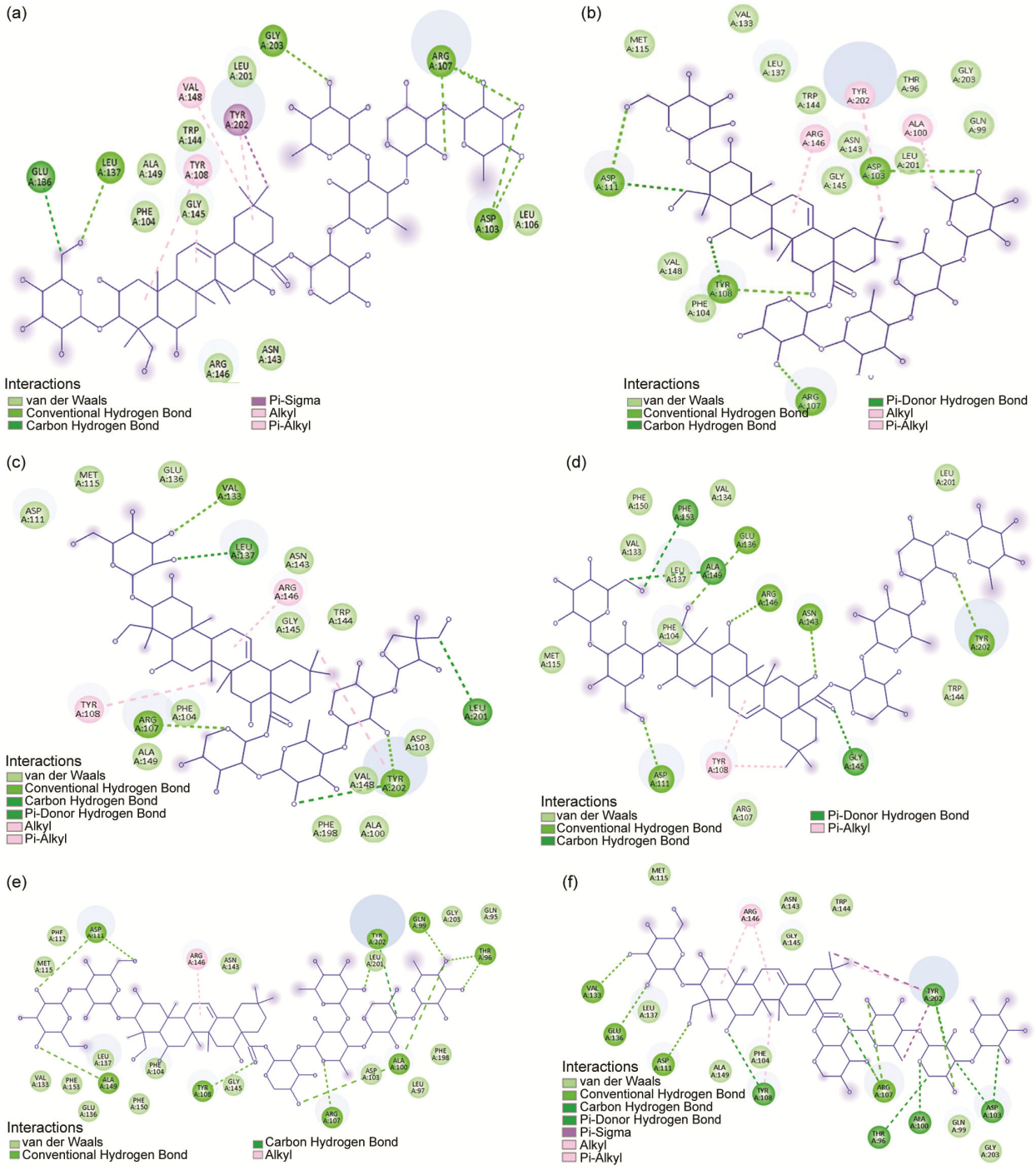

Fig. 7 — 2D interaction diagram between the 4G3F protein receptor and ligands. (a) CPD1, (b) CPD2, (c) CPD3, (d) CPD4, (e) CPD5, (f) CPD6, (g) CPD7, (h) CPD8, (i) CPD9, (j) CPD10, and (k) 5FU. (*Contd.*)

(*Contd.*)

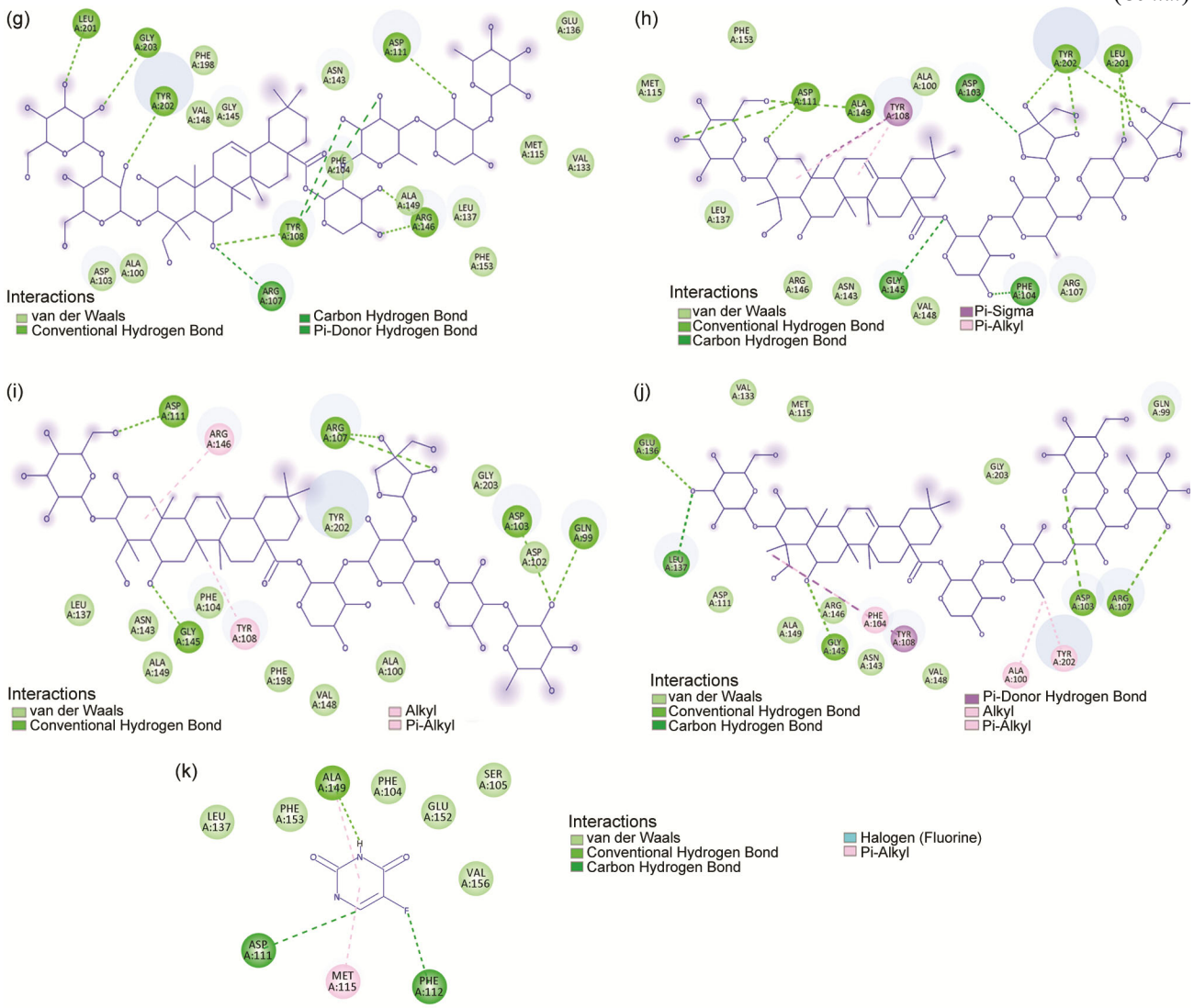

Fig. 7 — 2D interaction diagram between the 4G3F protein receptor and ligands. (a) CPD1, (b) CPD2, (c) CPD3, (d) CPD4, (e) CPD5, (f) CPD6, (g) CPD7, (h) CPD8, (i) CPD9, (j) CPD10, and (k) 5FU.

interactions result from the aggregation of non-polar entities in an aqueous milieu, reducing solvent exposure and fostering their association. Van der Waals forces contribute significantly to the stabilisation of protein-ligand complexes during docking, facilitating precise spatial orientation between interacting partners and enhancing binding affinity in synergy with hydrogen bonding and hydrophobic effects[29]. These noncovalent interactions prove essential for achieving an optimal docking configuration. A more negative binding energy typically signifies a more stable and favourable binding event, indicating enhanced ligand retention within the receptor[30].

These results indicate that CPD1 and CPD5, characterised by more negative binding energies (-10.5 kcal/mol and -10.38 kcal/mol) and a greater number of interactions (16 and 25 total, with 9 and 11 at active sites), display enhanced potential to inhibit 6QGG relative to 5FU (-3.5 kcal/mol, 10 interactions, 5 at active sites). The active sites Asp103, Leu137, and Tyr202, where CPD1 and CPD5 form robust interactions, play a vital role in modulating the anti-apoptotic activity of MCL-1, as structural data confirm their location within the BH3-binding pocket of the 6QGG structure[31]. These interactions likely disrupt the binding of pro-apoptotic proteins such as BAX and BAK, key steps in the apoptosis pathway,

thereby facilitating effective suppression of apoptosis resistance in prostate cancer cells. As noted in structural analyses, the observed conservation of these active sites across MCL-1 homologs supports their relevance for translational studies. Consequently, CPD1 and CPD5 emerge as promising candidates for subsequent molecular dynamics simulations, with 5FU serving as a reference compound to further evaluate the stability and dynamic behaviour of the ligand-protein complex within the MCL-1 binding pocket, particularly at these critical active sites.

Molecular dynamics simulations

Molecular dynamics (MD) simulations are a powerful tool for examining the behaviour of protein-ligand complexes over time, revealing conformational changes and assessing the stability of the interaction. These simulations provide a detailed, atomistic view of how a protein and a ligand interact, including how they move, change shape, and maintain their association[32]. This method follows molecular docking to confirm and enhance the outcomes derived from initial docking analyses. The evaluation systematically investigated RMSD, RMSF, Rg, hydrogen bond formation, and SASA metrics to determine the stability, flexibility, and solvent exposure of the CPD1-6QGG, CPD5-6QGG, and 5FU-6QGG complexes throughout the simulation timeframe.

The RMSD profiles for the CPD1-6QGG, CPD5-6QGG, and 5FU-6QGG complexes, monitored over an 80 ns simulation duration, exhibited distinct patterns (Fig. 8a). Specifically, the CPD1-6QGG complex displayed RMSD values fluctuating between 0.15 and 0.2 nm, with an average of 0.18 nm, suggesting a highly stable structural arrangement and a strong binding interaction with the 6QGG protein. Conversely, the CPD5-6QGG and 5FU-6QGG complexes showed RMSD values ranging from 0.2 to 0.3 nm, averaging 0.215 nm, indicating a marginally higher degree of structural flexibility while maintaining acceptable stability. This variation implies that CPD1-6QGG achieves a more consistent conformational stability than CPD5-6QGG and 5FU-6QGG, potentially reflecting a more favourable binding affinity within the 6QGG active site[33]. Thus, the observed RMSD trends support the conclusion that CPD1-6QGG retains its initial structure more effectively than CPD5-6QGG and 5FU-6QGG, as corroborated by the present dynamic assessment.

The RMSF represents a fundamental metric in molecular dynamics simulations, quantifying the average positional deviation of individual residues relative to a reference structure across the simulation period, thus reflecting their dynamic flexibility[34]. Fig. 8b depicts the RMSF profiles for the CPD1-6QGG, CPD5-6QGG, and 5FU-6QGG complexes, evaluated over an 80 ns simulation duration, with flexibility assessed across residues Ser8 to Gly203, encompassing the whole polypeptide chain of the 6QGG protein. This variability likely correlates with the spatial distribution of these residues relative to critical active binding sites, including key positions such as Asp103, Leu137, and Tyr202. Specifically, the CPD1-6QGG complex exhibits a decline in RMSF from 0.35 nm to 0.07 nm over the initial 0-50 residue range, followed by a stable plateau at 0.07 nm from residues 50 to 203, indicating a transition to consistent structural rigidity. Similarly, the CPD5-6QGG complex demonstrates a reduction in RMSF from 0.5 nm to 0.07 nm within the 0-50 residue segment, maintaining stability at 0.07 nm from residues 50 to 203, suggesting a comparable stabilisation trend. In contrast, the 5FU-6QGG complex decreases RMSF from 0.2 nm to 0.07 nm over the 0-50 residue range, stabilising at 0.07 nm from residues 50 to 203, reflecting a slightly less pronounced initial flexibility. This pattern suggests that 5FU-6QGG experiences a more moderate conformational adjustment compared to CPD1-6QGG and CPD5-6QGG. Consequently, the CPD1-6QGG and CPD5-6QGG complexes achieve greater structural consistency with reduced flexibility post-residue 50, highlighting their potential to regulate molecular interactions within the 6QGG protein active site effectively.

The Rg measures the compactness of a protein by calculating the root mean square distance of all atoms relative to the protein's centre of mass, thus serving as an indicator of its spatial organization[35]. A lower Rg value reflects a more compact conformation, while a higher Rg value indicates a more expanded structure. The assessment of Rg values for the complexes is depicted in Fig. 8c. The Rg values for the CPD1-6QGG, CPD5-6QGG, and 5FU-6QGG complexes displayed uniform fluctuations between 1.4 and 1.45 nm, with an average of approximately 1.42 nm over the 100 ns simulation duration, suggesting that all complexes sustain a consistently compact configuration of the 6QGG protein throughout the simulation timeframe.

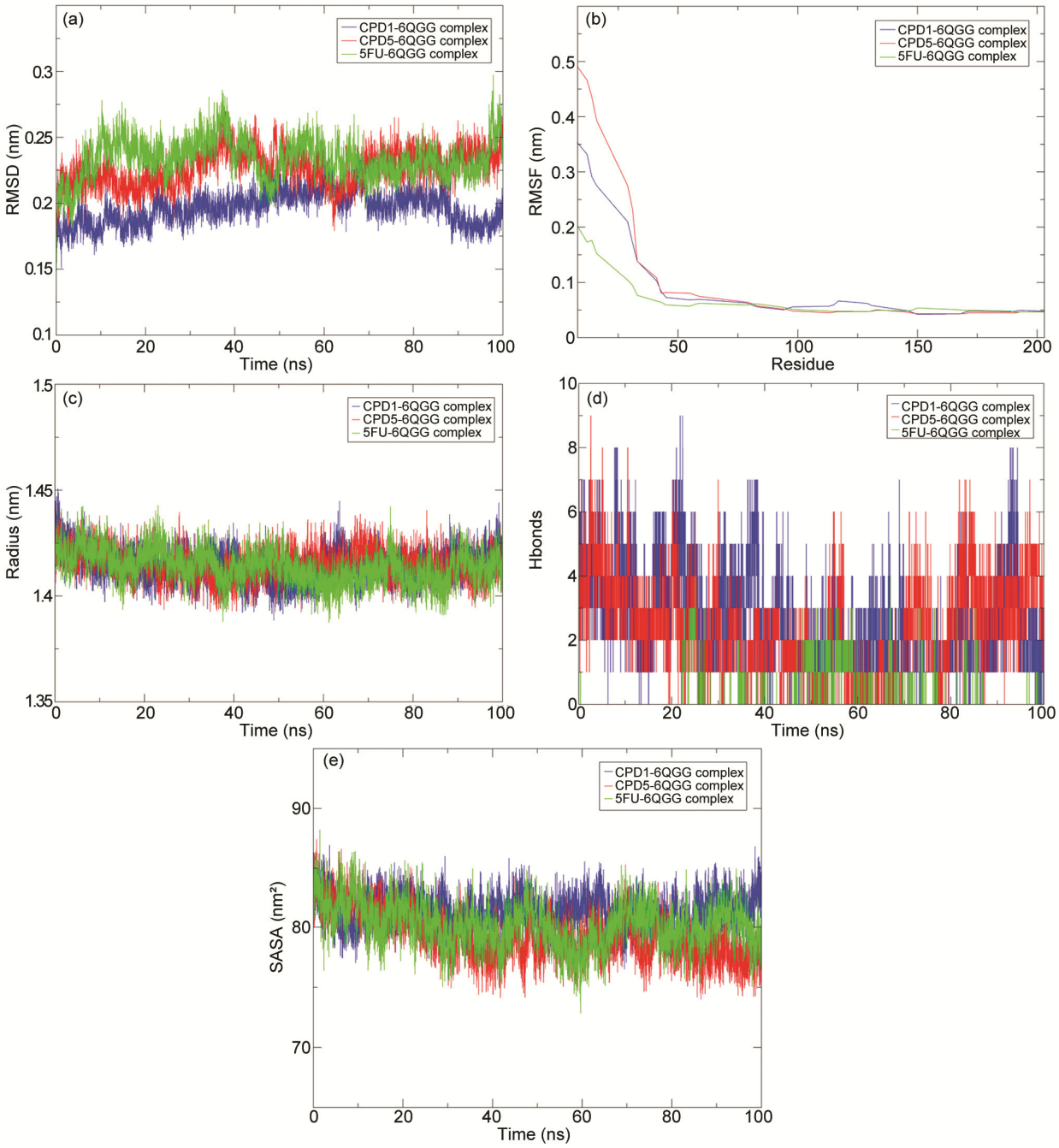

Fig. 8 — Molecular dynamics simulation results for the bindings of CPD1 (blue), CPD5 (red), and 5FU (green) with 6QGG protein. (a) RMSD, (b) RMSF, (c) Rg, (d) H-bonds, and (e) SASA.

Hydrogen bonds exert a significant influence in molecular dynamics simulations, profoundly impacting structural stability, conformational behaviour, and molecular interactions[36]. The presence of hydrogen bonds persisted throughout the simulation period, with the CPD1-6QGG complex exhibiting a range of 1 to 9 bonds, the CPD5-6QGG complex displaying 1 to 9 bonds, and the 5FU-6QGG complex showing 1 to 4 bonds. These findings suggest that all complexes maintain a stable association within the 6QGG protein binding site across the simulation timeframe, with the CPD1-6QGG and CPD5-6QGG complexes demonstrating a notably greater number of hydrogen bonds compared to the 5FU-6QGG complex (Fig. 8d). This disparity indicates that CPD1 and CPD5 foster a more extensive bonding network with the 6QGG protein.

The SASA measures the portion of a molecule's surface accessible to solvent molecules, typically modeled as spheres with a radius representing water molecules. This area is important in understanding molecular interactions, particularly in biological systems, as it relates to protein folding, ligand binding, and overall molecular dynamics[37]. The SASA values underwent evaluation to investigate the solvent exposure characteristics of the CPD1-6QGG, CPD5-6QGG, and 5FU-6QGG complexes. Analysis of the SASA profile indicated dynamic variations over the 100 ns simulation period, with all complexes exhibiting fluctuations between 75 and 87 nm^2, yielding an average value of approximately 80 nm^2 (Fig. 8e). These fluctuations suggest ligand-induced alterations in solvent accessibility, reflecting adaptations at the 6QGG-ligand interface that may influence binding characteristics. The consistency in fluctuation range and similar average values across the three complexes indicates a stable maintenance of the solvent-exposed surface, despite the markedly more favourable docking binding energies of CPD1 (-10.5 kcal/mol) and CPD5 (-10.38 kcal/mol) compared to 5FU (-3.5 kcal/mol), suggesting potential differences in binding interactions.

The thorough assessment of dynamic parameters has provided a detailed insight into the stability and structural characteristics of the CPD1-6QGG, CPD5-6QGG, and 5FU-6QGG complexes, emphasising the 6QGG protein's contribution to molecular interactions. The investigation revealed that the CPD1-6QGG and CPD5-6QGG complexes exhibit enhanced stability compared to the 5FU-6QGG complex's interaction with the 6QGG protein, identifying CPD1 and CPD5 as promising candidates. These results, aligned with the more favourable docking binding energies of CPD1 (-10.5 kcal/mol) and CPD5 (-10.38 kcal/mol) relative to 5FU (-3.5 kcal/mol), underscore their capacity to maintain robust binding with the 6QGG protein.

Free binding energy (MMGBSA) analysis

The binding free energies of the protein-ligand complexes were calculated through the MMGBSA method, as implemented in gmx_MMPBSA with the charmm36-jul2022.ff force field. Snapshots from the molecular dynamics simulation trajectories, encompassing the full 80 ns duration, underwent Molecular Mechanics/Generalized Born Surface Area (MM-GBSA) analysis. In the absence of the entropic contribution, the derived value constitutes the effective free energy, which suffices for relative comparisons of binding affinities among analogous systems. This investigation determined the effective free energy of binding across the entire 80 ns trajectory, utilising 125 snapshots extracted at 80 ps intervals (spanning 20 to 100 ns). This approach provided an average binding energy incorporating the dynamic characteristics of protein-ligand associations, thereby revealing the affinity and stability under simulated physiological conditions. MMGBSA values for all complexes are detailed in Table 3 and Fig. 9.

Table 3 — Free energy of binding obtained using MMGBSA calculations

Energy Component	Average (kcal/mol)			Standard Deviation		
	CPD1-6QGG	CPD5-6QGG	5FU-6QGG	CPD1-6QGG	CPD5-6QGG	5FU-6QGG
ΔBOND	-0.00	-0.00	-0.00	0.00	0.00	0.00
ΔANGLE	0.00	0.00	0.00	0.00	0.00	0.00
ΔDIHED	-0.00	-0.00	-0.00	0.00	0.00	0.00
ΔUB	0.00	0.00	0.00	0.00	0.00	0.00
ΔIMP	0.00	0.00	0.00	0.00	0.00	0.00
ΔCMAP	0.00	0.00	0.00	0.00	0.00	0.00
ΔVDWAΔALS	-44.56	-24.06	-5.91	4.44	8.21	5.83
ΔEEL	-39.25	-29.16	-6.95	22.46	28.18	10.53
Δ1-4 VDW	-0.00	-0.00	-0.00	0.00	0.00	0.00
Δ1-4 EEL	0.00	-0.00	0.00	0.00	0.00	0.00
ΔEGB	55.88	37.98	9.40	19.57	27.25	10.01
ΔESURF	-6.05	-3.28	-0.97	0.82	1.17	0.92
ΔGGAS	-83.81	-53.22	-12.87	24.78	33.08	14.16
ΔGSOLV	49.83	34.7	8.42	19.8	26.41	9.22

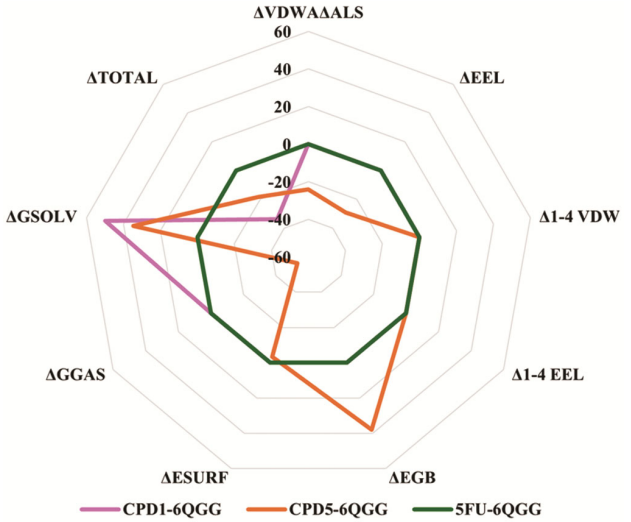

Fig. 9 — Comparison of individual MMGBSA energy values for all complexes.

For the examined systems, the effective free energy of binding yielded values of -33.98±7.04 kcal/mol for CPD1-6QGG, -18.52±9.32 kcal/mol for CPD5-6QGG, and -4.44±5.30 kcal/mol for 5FU-6QGG. The MMGBSA results indicated stronger binding for CPD1-6QGG relative to CPD5-6QGG and 5FU-6QGG, consistent with prior docking observations.

Conclusions

The study successfully integrated network pharmacology, molecular docking, and molecular dynamics simulations to explore triterpenoid saponins from *P. formosanum*, noted for their potential interaction with the 6QGG protein. The network pharmacology framework provided an initial platform for identifying plausible biological targets, while molecular docking analyses indicated that CPD1 and CPD5 display enhanced stability and precise alignment within the 6QGG binding site compared to 5FU. Molecular dynamics simulations over a 100 ns timeframe revealed a persistent interaction mechanism, with stable binding relationships between CPD1-6QGG and CPD5-6QGG, affirming a reliable and strong association with this apoptosis regulator. These results substantiate the ability of CPD1 and CPD5 to maintain effective interactions with 6QGG throughout the simulation period, highlighting their potential as MCL-1 inhibitors for targeting prostate cancer through apoptosis pathway modulation.

However, despite the promising computational insights, the importance of experimental validation to substantiate these findings remains paramount. Due to the unavailability of experimental facilities, this study excluded *in vitro* and *in vivo* assessments. Future investigations should prioritise laboratory-based evaluations to examine the interaction characteristics of CPD1 and CPD5 thoroughly. Such studies should investigate the compounds' impact on cellular models, establishing their therapeutic efficacy and safety attributes. The absence of experimental data and the lack of analysis regarding potential covalent inhibition constitute limitations of the current research. Should preclinical evaluations affirm the potential of CPD1 and CPD5, they may merit consideration for further clinical development. Although additional studies are necessary to expand knowledge, the present findings lay a solid groundwork for future research and offer a promising avenue for therapeutic advancement.

Conflict of interest

The authors have no competing interests to declare that are relevant to the content of this article.

AI use disclosure

During the preparation of this work, the author used Grammarly and Google Translate in order to improve language quality, correct grammar and spelling errors, and assist with translation during the writing process. After using these tools/services, the author reviewed and edited the content as needed and takes full responsibility for the content of the published article.

References

1 Bray F, Laversanne M, Sung H, Ferlay J, Siegel R L, *et al.*, Global cancer statistics 2022: GLOBOCAN estimates of incidence and mortality worldwide for 36 cancers in 185 countries, *CA Cancer J Clin*, 2024, **74**(3), 229–263, doi: 10.3322/caac.21834.

2 Wilson T K and Zishiri O T, Prostate cancer: a review of genetics, current biomarkers and personalised treatments, *Cancer Rep*, 2024, **7**(10), e70016, doi: 10.1002/cnr2.70016.

3 Aragon-Ching J B and Dahut W L, Novel androgen deprivation therapy (ADT) in the treatment of advanced prostate cancer, *Drug Discov Today Ther Strateg*, 2010, **7**(1), 31–35, doi: 10.1016/j.ddstr.2011.02.004.

4 Gebauer J, Higham C, Langer T, Denzer C and Brabant G, Long-term endocrine and metabolic consequences of cancer treatment: a systematic review, *Endocr Rev*, 2019, **40**(3), 711–767, doi: 10.1210/er.2018-00092.

5 Tan B Y, Lin H, Zhang H G, Zhao J Z, Deng S Y, *et al.*, Cytotoxic monoterpenoid indole alkaloids from *Tabernaemontana bovina*, *Phytochemistry*, 2025, **230**, 114336, doi: 10.1016/j.phytochem.2024.114336.

6 Bousbaa H, Cidade H and Silva P M A, Advances in bioactive compounds and cancer therapy-insights from the

special issue "Bioactive compounds in cancers", *Int J Mol Sci*, 2025, **26**(12), 5632, doi: 10.3390/ijms26125632.

7 Majnooni M B, Fakhri S, Ghanadian S M, Bahrami G, Mansouri K, *et al.*, Inhibiting angiogenesis by anticancer saponins: from phytochemistry to cellular signaling pathways, *Metabolites*, 2023, **13**(3), 323, doi: 10.3390/metabo13030323.

8 Bildziukevich U, Wimmerová M and Wimmer Z, Saponins of selected triterpenoids as potential therapeutic agents: a review, *Pharmaceuticals*, 2023, **16**(3), 386, doi: 10.3390/ph16030386.

9 Menchinskaya E S, Dyshlovoy S A, Venz S, Jacobsen C, Hauschild J, *et al.*, Anticancer activity of the marine triterpene glycoside cucumarioside a2-2 in human prostate cancer cells, *Mar Drugs*, 2024, **22**(1), 20, doi: 10.3390/md22010020.

10 Sachan R, Kundu A, Jeon Y, Choi W S, Yoon K, *et al.*, Afrocyclamin A, a triterpene saponin, induces apoptosis and autophagic cell death via the PI3K/Akt/mTOR pathway in human prostate cancer cells, *Phytomedicine*, 2018, **51**, 139–150, doi: 10.1016/j.phymed.2018.10.012.

11 Chen H Y, Liu J F, Tsai S F, Lin Y L and Lee S S, Cytotoxic protobassic acid saponins from the kernels of *Palaquium formosanum*, *J Food Drug Anal*, 2018, **26**(2), 557–564, doi: 10.1016/j.jfda.2017.06.004.

12 Keiser M J, Roth B L, Armbruster B N, Ernsberger P, Irwin J J, *et al.*, Relating protein pharmacology by ligand chemistry, *Nat Biotechnol*, 2007, **25**(2), 197–206, doi: 10.1038/nbt1284.

13 Szklarczyk D, Gable A L, Nastou K C, Lyon D, Kirsch R, *et al.*, The STRING database in 2021: customizable protein–protein networks, and functional characterization of user-uploaded gene/measurement sets, *Nucleic Acids Res*, 2021, **49**(D1), D605–D612, doi: 10.1093/nar/gkaa1074.

14 Clarke D J B, Kuleshov M V, Schilder B M, Torre D, Duffy M E, *et al.*, eXpression2Kinases (X2K) Web: linking expression signatures to upstream cell signaling networks, *Nucleic Acids Res*, 2018, **46**(W1), W171–W179, doi: 10.1093/nar/gky458.

15 Nguyen H D, Molecular docking and dynamic simulation of anti-apoptotic BCL-2 with saponins isolated from *Weigela* x "Bristol Ruby", *Indian J Chem*, 2025, **64**(4), 383–390, doi: 10.56042/ijc.v64i4.15530.

16 Murray J B, Davidson J, Chen I, Davis B, Dokurno P, *et al.*, Establishing drug discovery and identification of hit series for the anti-apoptotic proteins, Bcl-2 and Mcl-1, *ACS Omega*, 2019, **4**(5), 8892–8906, doi: 10.1021/ acsomega.9b00611.

17 Laskowski R A, MacArthur M W, Moss D S and Thornton J M, PROCHECK: a program to check the stereochemical quality of protein structures, *J Appl Crystallogr*, 1993, **26**(2), 283–291, doi: 10.1107/S0021889892009944.

18 Van Der Spoel D, Lindahl E, Hess B, Groenhof G, Mark A E, *et al.*, GROMACS: fast, flexible, and free, *J Comput Chem*, 2005, **26**(16), 1701–1718, doi: 10.1002/jcc.20291.

19 Guex N and Peitsch M C, SWISS-MODEL and the Swiss-Pdb Viewer: an environment for comparative protein modeling, *Electrophoresis*, 1997, **18**(15), 2714–2723, doi: 10.1002/elps.1150181505.

20 Zoete V, Cuendet M A, Grosdidier A and Michielin O, SwissParam: a fast force field generation tool for small organic molecules, *J Comput Chem*, 2011, **32**(11), 2359–2368, doi: 10.1002/jcc.21816.

21 Pettersen E F, Goddard T D, Huang C C, Couch G S, Greenblatt D M, *et al.*, UCSF Chimera-a visualization system for exploratory research and analysis, *J Comput Chem*, 2004, **25**(13), 1605–1612, doi: 10.1002/jcc.20084.

22 Genheden S and Ryde U, The MM/PBSA and MM/GBSA methods to estimate ligand-binding affinities, *Expert Opin Drug Discov*, 2015, **10**(5), 449–461, doi: 10.1517/17460441.2015.1032936.

23 Farooq M, Khan A W, Kim M S and Choi S, The role of fibroblast growth factor (FGF) signaling in tissue repair and regeneration, *Cells*, 2021, **10**(11), 3242, doi: 10.3390/cells 10113242.

24 Hu X, li J, Fu M, Zhao X and Wang W, The JAK/STAT signaling pathway: from bench to clinic, *Signal Transduct Target Ther*, 2021, **6**(1), 402, doi: 10.1038/s41392-021-00791-1.

25 Ghalehbandi S, Yuzugulen J, Pranjol M Z I and Pourgholami M H, The role of VEGF in cancer-induced angiogenesis and research progress of drugs targeting VEGF, *Eur J Pharmacol*, 2023, **949**, 175586, doi: 10.1016/j.ejphar.2023.175586.

26 Forli S, Huey R, Pique M E, Sanner M F, Goodsell D S, *et al.,* Computational protein–ligand docking and virtual drug screening with the AutoDock suite, *Nat Protoc*, 2016, **11**(5), 905–919, doi: 10.1038/nprot.2016.051.

27 Ramírez D and Caballero J, Is it reliable to take the molecular docking top scoring position as the best solution without considering available structural data?, *Molecules*, 2018, **23**(5), 1038, doi: 10.3390/molecules23051038.

28 Mahamba L, Isa M A and Kappo A P, *In silico* identification of potential inhibitors for the universal stress G4LZI3 protein from *Schistosoma mansoni* using molecular docking and molecular dynamics simulation analyses, *Asp Mol Med*, 2025, **5**, 100084, doi: 10.1016/j.amolm.2025.100084.

29 Yao W, Mo L, Fang L and Qin L, Molecular dynamics simulations on interactions of five antibiotics with luciferase of *Vibrio Qinghaiensis* sp-Q67, *Ecotoxicol Environ Saf*, 2023, **256**, 114910, doi: 10.1016/j.ecoenv.2023.114910.

30 Bitencourt-Ferreira G, Veit-Acosta M and de Azevedo W F, in *Docking screens for drug discovery*, edited by de Azevedo W F, (Springer, New York), 2019, 79–91.

31 Tantawy S I, Timofeeva N, Hernandez A, Sarkar A and Gandhi V, Decoding the mechanism behind MCL-1 inhibitors: a pathway to understanding MCL-1 protein stability, *Oncotarget*, 2023, **14**, 653, doi: 10.18632/oncotarget.28440.

32 Sasidharan S, Gosu V, Tripathi T and Saudagar P, in *Protein folding dynamics and stability: experimental and computational methods*, edited by Saudagar P & Tripathi T, (Springer Nature, Singapore), 2023, 107–127.

33 Kufareva I and Abagyan R, in *Homology modeling: methods and protocols*, edited by Orry A J W & Abagyan R, (Humana Press, Totowa), 2012, 231–257.

34 Sharma J, Kumar Bhardwaj V, Singh R, Rajendran V, Purohit R, *et al.*, An *in-silico* evaluation of different bioactive molecules of tea for their inhibition potency against non structural protein-15 of *SARS-CoV-2*, *Food Chem*, 2021, **346**, 128933, doi: 10.1016/j.foodchem.2020.128933.

35 Victorien Hermann H D, Jules F J and Jeanet C, Novel agents inhibiting the Marburg nucleoprotein using molecular docking, ADMET, MD, and quantum DFT methods, *Discov Appl Sci*, 2025, **7**(7), 749, doi: 10.1007/s42452-025-07356-9.

36 Ferenczy G G and Kellermayer M, Contribution of hydrophobic interactions to protein mechanical stability, *Comput Struct Biotechnol J*, 2022, **20**, 1946–1956, doi: 10.1016/j.csbj.2022.04.025.

37 Durham E, Dorr B, Woetzel N, Staritzbichler R and Meiler J, Solvent accessible surface area approximations for rapid and accurate protein structure prediction, *J Mol Model*, 2009, **15**(9), 1093–1108, doi: 10.1007/s00894-009-0454-9.